Original Article

SHM Structural Health Monitoring

Structural Health Monitoring
2017, Vol. 16(1) 62–78

DOI: 10.1177/1475921716662142
shm.sagepub.com
SAGE

On the application of discrete-time Volterra series for the damage detection problem in initially nonlinear systems

Sidney B Shiki[1], Samuel da Silva[1] and Michael D Todd[2]

Abstract

Nonlinearities in the dynamical behavior of mechanical systems can degrade the performance of damage detection features based on a linearity assumption. In this article, a discrete Volterra model is used to monitor the prediction error of a reference model representing the healthy structure. This kind of model can separate the linear and nonlinear components of the response of a system. This property of the model is used to compare the consequences of assuming a nonlinear model during the nonlinear regime of a magneto-elastic system. Hypothesis tests are then employed to detect variations in the statistical properties of the damage features. After these analyses, conclusions are made about the application of Volterra series in damage detection.

Keywords

Damage detection, nonlinear dynamics, discrete-time Volterra series, statistical hypothesis testing, system identification

Introduction

Nonlinear behavior is commonly present in mechanical systems such that linear tools can drastically fail to describe the complex dynamics of these structures.[1] A few typical sources of nonlinearity are geometric nonlinearities, gaps, bolted connections, clearance, gaps, impacts, cracks, materials with nonlinear constitutive relationship, and so on.[2] As a consequence, even simple systems can exhibit complex nonlinear responses containing harmonic distortion, jumps, modal interactions, bifurcation, and chaos.[3] These effects can be a great problem when monitoring a system during the nonlinear regime of operation.[4]

The structural health monitoring (SHM) literature deals with nonlinear structures in basically two approaches. In the first one, the system is considered to be linear and damage subsequently induces a nonlinearity in the structural response.[5] This is an appealing strategy since typical fault modes like cracks, impacts, delamination, and rubbing of rotating machinery induce nonlinearity. In this kind of situation, the identification of structural changes can be viewed as a procedure for detection of nonlinearities in the measured response of the system. Many well-established nonlinear tools such as coherence function, Hilbert transform, higher order spectra, and phase-space methods can be employed in this case.[6,7] Many recent papers still explore nonlinearity with features based on modal properties,[8] wave propagation,[9] and signal processing techniques[10] usually taking advantage of the fact that the damage is in many cases a source of nonlinear behavior.

In the second approach, the system is considered to be nonlinear before the occurrence of the damage.[11] In this case, it is necessary to appropriately model the baseline behavior of the structure in a way that the inherent nonlinear effects of the system are not mistakenly viewed as damage. In this case, techniques such as the restoring force surface method, nonlinear autoregressive models, autoregressive support vector machines, Hilbert transform, principal component analysis, and time–frequency analyses, among others, may be applied to detect and quantify such

[1]Departamento de Engenharia Mecânica, Faculdade de Engenharia, UNESP—Universidade Estadual Paulista, Ilha Solteira, Brasil
[2]Department of Structural Engineering, University of California, San Diego, La Jolla, CA, USA

Corresponding author:
Samuel da Silva, Departamento de Engenharia Mecânica, Faculdade de Engenharia, UNESP—Universidade Estadual Paulista, Av. Brasil, 56, 15385-000 Ilha Solteira, SP, Brasil.
Email: samuel@dem.feis.unesp.br

nonlinearity.[2,7,11–13] However, there is still no general model to deal with nonlinear dynamics in a comprehensive way and the application of mathematical tools in nonlinear problems tends to be case-specific.[2]

Among the existent tools for nonlinear system identification, Volterra series is a promising model class since it is a generalization of the linear convolution representing the linear and nonlinear responses of a dynamical system in a separable way.[14,15] The main challenges in the application of this model are in the calculation of the generalized impulse response functions, named Volterra kernels. The most popular approach in structural dynamics is called harmonic probing.[1] This estimation method consists in probing a nonlinear system with harmonic signals in order to calculate the kernels in the frequency domain, also called higher order frequency response functions (HOFRFs). The main limitation of this formulation is that the motion equation or some discrete-time model of the system (e.g. autoregressive models) should be known a priori in order to obtain the analytical HOFRFs.[16] Despite this limitation, the harmonic probing already has had successful applications in nonlinear system identification[17] and damage detection.[18]

Other possible way to deal with the identification of Volterra kernels is to use input and output information of the nonlinear system. This is a practical approach since it is easier to apply it together with data collected in an experimental test during the nonlinear regime of the structure. This kind of technique was already applied in the aeroelasticity literature in order to obtain reduced models instead of using traditional computational fluid dynamics models that are computationally intensive.[19] The authors of this article also have done applications of discrete-time Volterra series for system identification,[20,21] model updating,[22] and damage detection[23] for simulated nonlinear structures. Alleged problems of convergence and overparameterization that can appear in the use of this model[24] can be minimized by expanding Volterra kernels with orthonormal functions[21] or wavelet bases.[25]

A few papers have already explored the interesting properties of Volterra models in applications for damage detection. One of the first articles to utilize Volterra series expansion with damage identification problems was done by Ruotolo et al.,[26] which simulated a cantilever beam with a closing crack using a nonlinear finite element model. The response of the model was used to estimate the main diagonals of the HOFRFs using a stepped sine testing. The authors demonstrated the usefulness of this representation to show the sensitivity of the nonlinear HOFRFs to the size and position of the crack. Peng et al.[27] used nonlinear output frequency response functions (NOFRFs) which is a concept based on Volterra series to detect nonlinear components in a periodic structure. This approach can be used in damage detection for the cases when the damage is a source of nonlinearity. Surace et al.[28] show the effects of cracks in the HOFRFs which are represented as a bilinear nonlinearity. The authors calculated the HOFRFs by the probing method and they showed that the nonlinear kernels are much more sensitive to the crack parameters. In a similar problem, Chatterjee[18] uses the HOFRFs to calculate the components of the response of a beam with breathing crack. Rébillat et al.[29] apply Hammerstein models using damage features based on nonlinear components of the response in order to detect damage. The method is applied in linear systems subjected to a bilinear nonlinearity that represents a crack in the system. The technique is also applied to detect impact damage in a composite plate. Tang et al.[30] use a damage metric based on the Volterra kernels identified with acceleration data from a rotor-bearing system. When considering a model with the first three kernels, it was able to separate the healthy system to the unbalanced and rubbing conditions.

In this article, the Volterra representation is used to build a model representing a magneto-elastic system with a bolted connection. In this structure, nonlinearity appears when large displacements are induced in the system intensifying the magnetic forces of the permanent magnet on the beam. Damage is simulated by removing small masses in the connection. The prediction error of the model is used together with statistical hypothesis testing in order to detect structural variations in the linear and nonlinear regime of operation of the system. This research contributes to the SHM literature by providing a method for damage detection that can be used to verify structural variations even during the nonlinear regime of motion. Also, the article aims to show the possible consequences of assuming linearity in a simple experimental setup by comparing the nonlinear model with its equivalent linear version. The discrete Volterra model is employed in this article due to the stability for a bounded input[31] (bounded input bounded output (BIBO) stable) and because it is a nonparametric model that does not require a previous model or information about the system.[32] Also, it is a useful option for the problem of detection of structural variations in nonlinear systems because it can represent the linear and nonlinear responses as separable terms.[33] This allows one to propose equivalent linear and nonlinear indexes that are used in this article to make clear the drawbacks of using linear damage features.

The content of the article is divided in six main sections. In the second section, the basics of Volterra kernels identification are briefly presented. The third section shows the methodology of damage detection as well as the hypothesis test used in this work. The fourth section presents the nonlinearity detection,

characterization, and identification of the experimental Volterra kernels. The fifth section shows the application of the identified model to detect structural changes. Finally, the final remarks are made in the sixth section.

Discrete-time Volterra series

In the discrete-time Volterra model, the kth sample of the response of the system is described by an infinite sum of a linear component $y_1(k)$ and the nonlinear components $y_2(k) + y_3(k) + \cdots$[14,15]

$$y(k) = \sum_{\eta=1}^{+\infty} y_\eta(k) = y_1(k) + y_2(k) + y_3(k) + \cdots \quad (1)$$

In the Volterra series expansion, each η-order term of the response may be expressed as a multidimensional convolution between the Volterra kernels $\mathcal{H}_\eta(n_1, \ldots, n_\eta)$ and the input signal $u(k)$[31]

$$y_\eta(k) = \sum_{n_1=0}^{N_\eta-1} \cdots \sum_{n_\eta=0}^{N_\eta-1} \mathcal{H}_\eta(n_1, \ldots, n_\eta) \prod_{i=1}^{\eta} u(k-n_i) \quad (2)$$

where $N_1, \ldots, N_\eta$ are the memory lengths of each ηth kernel through its different dimensions. By analyzing the first-order term, it is possible to observe that it corresponds to the linear convolution sum

$$y_1(k) = \sum_{n_1=0}^{N_1-1} \mathcal{H}_1(n_1) u(k-n_1) \quad (3)$$

Meanwhile, the higher order responses are generalizations of the linear portion of the response and have similar expressions to the linear equivalent. The second- and third-order terms are illustrated in equations (4) and (5), respectively

$$y_2(k) = \sum_{n_1=0}^{N_2-1} \sum_{n_2=0}^{N_2-1} \mathcal{H}_2(n_1, n_2) u(k-n_1) u(k-n_2) \quad (4)$$

$$y_3(k) = \sum_{n_1=0}^{N_3-1} \sum_{n_2=0}^{N_3-1} \sum_{n_3=0}^{N_3-1} \mathcal{H}_3(n_1, n_2, n_3) u(k-n_1) u(k-n_2) u(k-n_3) \quad (5)$$

However, the main issue with this model is the very large number of terms that are needed to represent a nonlinear system response.[21] This is especially relevant in the case of the higher order terms, which have additional dimensions. A way to overcome these limitations is to represent the Volterra kernels using an approximation with orthonormal functions $\psi_{i_j}(n_j)$[25,34]

$$\mathcal{H}_\eta(n_1, \ldots, n_\eta) \approx \sum_{i_1}^{J_\eta} \cdots \sum_{i_\eta}^{J_\eta} \mathcal{B}_\eta(i_1, \ldots, i_\eta) \prod_{j=1}^{\eta} \psi_{i_j}(n_j) \quad (6)$$

where $\mathcal{B}_\eta(i_1, \ldots, i_\eta)$ are the orthonormal projections of the Volterra kernels and $J_1, \ldots, J_\eta$ are the number of samples in each orthonormal projection. This representation has the advantage of drastically reducing the number of samples in the orthonormal expression when an appropriate basis function is selected. This fact improves the speed of the calculation of the multidimensional convolutions and in the computation of the Volterra kernels. By assuming the orthonormal representation of the kernels, it is possible to define the input signal as being filtered by the orthonormal functions

$$l_{i_j}(k) = \sum_{n_i}^{V-1} \psi_{i_j}(n_i) u(k-n_i) \quad (7)$$

where $l_{i_j}(k)$ is the filtered input signal and $V = \max\{J_1, \ldots, J_\eta\}$. With this new variable the η-order response can be written as

$$y_\eta(k) \approx \sum_{i_1=1}^{J_\eta-1} \cdots \sum_{i_\eta=1}^{J_\eta-1} \mathcal{B}_\eta(i_1, \ldots, i_\eta) \prod_{j=1}^{\eta} l_{i_j}(k) \quad (8)$$

Provided that an input and output signal were measured in an experimental test in the system, it is possible to apply a simple least-squares approximation in order to estimate the Volterra kernels until the order η in which the model was truncated[31]

$$\mathbf{\Phi} = \left(\mathbf{\Gamma}^T \mathbf{\Gamma}\right)^{-1} \mathbf{\Gamma}^T \mathbf{y} \quad (9)$$

where $\mathbf{\Phi}$ is a vector containing the orthonormal versions of the kernels until the considered order η, $\mathbf{\Gamma}$ is a matrix with combinations of the convolved input signals $l_{i_j}(k)$, and $\mathbf{y}$ is a vector with the captured sampled outputs. However, in the application of equation (9), it is necessary that the input signal can really excite the nonlinear higher order terms of the system. Commonly used signals in modal testing such as impact and sine excitations are not able to excite all the terms in the Volterra kernels,[31] while random excitation is not an effective way to activate nonlinearities.[1] In this article, the Volterra kernels were calculated using a chirp input signal that was able to show harmonics in the response and the hardening effect in the frequency domain. By calculating the vector $\mathbf{\Phi}$, it is possible to retrieve the assumed orthonormal kernels $\mathcal{B}_\eta(i_1, \ldots, i_\eta)$ that can be used to calculated the components of the Volterra model response $y_\eta(k)$. Appendix 1 shows the construction of the matrices $\mathbf{\Gamma}$ and $\mathbf{\Phi}$ in detail.

However, in order to have a representative model of the nonlinear system, a properly chosen orthonormal function basis has to be applied in the expansion illustrated in equation (6). In the case of oscillatory systems, it is usual to use Kautz orthonormal functions, which can be described in the discrete frequency domain as a pair of functions $\Psi_{\eta,2g}(z)$ and $\Psi_{\eta,2g-1}(z)$

$$\Psi_{\eta,2g}(z)=\frac{\sqrt{\left(1-d_\eta^2\right)\left(1-b_\eta^2\right)}z}{z^2+b_\eta(d_\eta-1)z-d_\eta}\left[\frac{-d_\eta z^2+b_\eta(d_\eta-1)z+1}{z^2+b_\eta(d_\eta-1)z-d_\eta}\right]^{g-1} \tag{10}$$

$$\Psi_{\eta,2g-1}(z)=\frac{z-b_\eta}{\sqrt{1-b_\eta^2}}\Psi_{2g}(z) \tag{11}$$

where z is the complex variable in the discrete domain, g is an index such that $g\in[1,2,\ldots,J_\eta/2]$, and b_η and d_η can be obtained by

$$b_\eta=\frac{\left(Z_\eta+\bar{Z}_\eta\right)}{\left(1+Z_\eta\bar{Z}_\eta\right)} \tag{12}$$

$$d_\eta=-Z_\eta\bar{Z}_\eta \tag{13}$$

where Z_η and $\bar{Z}_\eta$ are the pair of conjugate poles that are the parameters of the Kautz functions. Note that the mentioned time-domain orthonormal functions $\psi_{i_j}(n_j)$ are the impulse response functions of the frequency-domain version of the Kautz functions $\Psi_{\eta,2g}(z)$ and $\Psi_{\eta,2g-1}(z)$. The poles of these functions have to be determined in order to represent the Volterra kernels. The discrete poles Z_η can be related to the continuous poles S_η through the equation

$$Z_\eta=\exp\left(\frac{S_\eta}{F_s}\right) \tag{14}$$

where F_s is the sampling frequency used in the discretization of the time-domain signals. The continuous poles of the Kautz functions can be related to the ηth natural frequency ω_η and damping ratio ς_η through

$$S_\eta=-\zeta_\eta\omega_\eta+j\omega_\eta\sqrt{1-\zeta_\eta^2} \tag{15}$$

In the case of oscillatory systems, the Kautz function representing the ηth Volterra kernel can be represented by the parameters ω_η and ς_η which are usually close to the parameters describing the linear dynamics of the system.[21] The next section shows the application of this model as a reference of the nonlinear system in the healthy condition in order to detect structural variations.

Damage detection methodology

Using the methodology described in the previous section, it is possible to identify a model of a nonlinear system using input and output data to estimate the Volterra kernels. Assuming that the identified Volterra kernels can represent the response of the system in the reference structural condition, it is possible to use this model to detect discrepancies in the measured output of a nonlinear structure that might be caused by damage. One simple way to perform this task is to analyze the prediction error of the model. Since the Volterra model is a series expansion, it is possible to obtain prediction errors considering different numbers of terms in the expansion

$$e_\eta=y_{exp}-\sum_{m=1}^{\eta}y_m \tag{16}$$

where e_η is the η-order prediction error, y_{exp} is the measured response, and the sum represents the response of the model with order η. It can be interesting to analyze a purely linear error (for $\eta=1$) and compare with the error considering higher order terms of the model. This can show the drawbacks of considering a linear model when monitoring a structure under the nonlinear regime of response. In order to have a lower dimension, feature to analyze a damage index can be used based on the ratio between the standard deviation of the prediction errors in the unknown structural condition and in the reference state

$$\lambda_\eta=\frac{\sigma\left(e_{\eta,unk}\right)}{\sigma\left(e_{\eta,ref}\right)} \tag{17}$$

where λ_η is the η-order damage index; $e_{\eta,unk}$ and $e_{\eta,ref}$ are, respectively, the η-order prediction errors in the unknown and reference states; and σ is the standard deviation operator. A similar index was already applied in the paper of Sohn and Farrar[35] for the detection of nonlinear damage in an experimental system with 8 degrees of freedom.

The expected statistical distribution of this variable can be determined by assuming a Gaussian distribution in the prediction errors. With this assumption, it is possible to relate equation (17) to an F distribution which describes the ratio between the variances of two variables.[36] This distribution can be modified by a simple change of variables which gives

$$P(\lambda)=\frac{2\left[\frac{\nu_1}{\nu_2}\right]^{\frac{\nu_1}{2}}\lambda^{\nu_1-1}}{\beta\left(\frac{\nu_1}{2},\frac{\nu_2}{2}\right)\left[1+\frac{\nu_1}{\nu_2}\lambda^2\right]^{\left(\frac{\nu_1+\nu_2}{2}\right)}} \tag{18}$$

where $P(\lambda)$ is the probability density function of the λ index and v_1 and v_2 are the number of degrees of freedom for the prediction errors in the unknown and reference states, respectively. In this case, these degrees of freedom can be calculated by $v_1 = m_1 - 1$ and $v_2 = m_2 - 1$ where m_1 and m_2 are the number of samples in $e_{\eta,unk}$ and $e_{\eta,ref}$, respectively. The term β is a function

$$\beta(a,b) = \frac{(a-1)!(b-1)!}{(a+b-1)!} \tag{19}$$

where a and b are the arguments of the β function. With the knowledge of the distribution of the index, it is possible to apply a statistical hypothesis test in order to detect a significant increase in the prediction error under a significance level α

$$\begin{aligned} H_0 &: \sigma(e_{\eta,unk}) = \sigma(e_{\eta,ref}) \\ H_1 &: \sigma(e_{\eta,unk}) > \sigma(e_{\eta,ref}) \end{aligned} \tag{20}$$

where H_0 is the null hypothesis and H_1 is the alternative hypothesis. In this formulation, H_0 is the condition where it is likely that the system is still in the reference condition. Meanwhile, H_1 represents the case where a significant increase in the prediction error is detected. One must note here that the type of change in the system that causes the increase in the error is not specified in equation (20). In practice, this means that the proposed method is assuming that no other effects other than changes in the structure are affecting the response of the system.

In order to classify a certain system between damaged and undamaged, the experimental input and output u_{unk} and y_{unk} are measured and the reference Volterra model is used to calculate the expected response of the system in the reference state. With the prediction errors in the unknown state $e_{\eta,unk}$ and in the reference state $e_{\eta,ref}$, the λ_η index is calculated with equation (17). Using this value, it is possible to calculate the probability of the observed λ_η to happen in the case where H_0 is true. This probability is usually named the p value and can be calculated assuming a right-tailed test as[37]

$$p = 1 - \int_0^{\lambda_\eta} P(\lambda)\, d\lambda \tag{21}$$

where the integral represents the area under the $P(\lambda)$ curve, also called the cumulative distribution function (CDF). In this sense, the p value for this right-tailed test is the probability of λ_η or higher values to be found in cases where the structure is in the reference state. In this case, the results of this statistical test can be divided in two possible conclusions:

- $p > \alpha$. It means that one is likely to observe the calculated sample λ_η when there is no structural variation. In other words, the null hypothesis H_0 cannot be rejected (no damage) for the considered value of α.
- $p < \alpha$. In this case, one is not likely to observe the sample λ_η when there is no structural variation. This means that H_0 should be rejected (damage) for the considered value of the significance level α.

This analysis is applied in an experimental example with a simple nonlinear system during the linear and nonlinear regime of operation of the structure.

Nonlinearity detection and system identification

In this section, an experimental example is described and a reference Volterra model representing the healthy structure is identified using input and output data measured during a modal testing. This model is later used to detect structural variations in the system using the statistical test described previously.

Nonlinear behavior of the system

The experimental setup is composed by a cantilever aluminum beam with dimensions of 300 mm × 19 mm × 3.2 mm. This beam has a steel mass attached to the free end and a neodymium magnet positioned 2 mm from the mass. A bolted connection is placed 150 mm from the free end with four nuts with nearly 1 g each in order to simulate structural variations for the damage detection investigation. An electrodynamic shaker is attached 50 mm away from the clamped end instrumented with a load cell. A laser vibrometer is used to measure the velocity on the free end of the beam. A schematic diagram and a picture of the experimental setup are illustrated in Figures 1 and 2.

The nonlinear behavior in this system comes from the magnetic interactions between the permanent magnet and the steel mass placed in the free end of the beam. The beam is positioned in a way that it is stretched in the axial direction and also attracts the tip of the beam during the bending movement causing a hardening effect in the system when large displacements occur in the free end.

In order to detect and visualize the nonlinear effects in the system, a chirp and stepped sine input signals were used to excite the structure with the shaker under different amplitudes. The signals of force and velocity

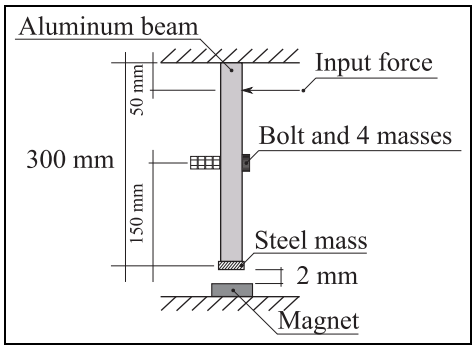

Figure 1. Schematic diagram of the experimental setup.

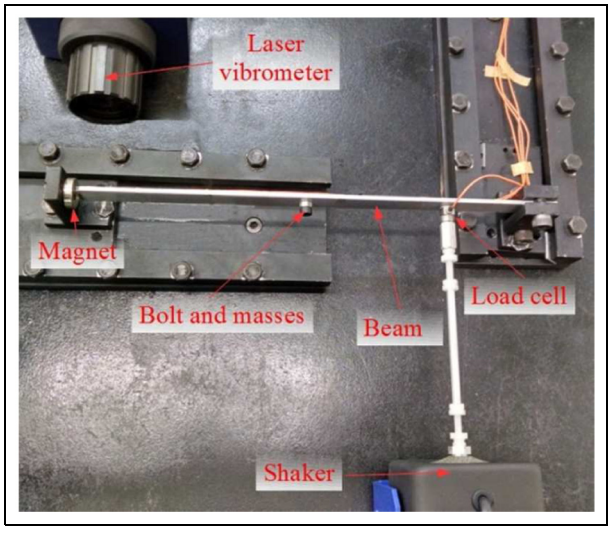

Figure 2. Picture of the experimental setup.

measured in the setup were captured using a 1024-Hz sampling rate. The chirp input was set to sweep up the range from 10 to 50 Hz around the first mode with 4096 samples using three different voltage levels applied in the shaker: 0.01, 0.10, and 0.15 V. With the input force measured by the load cell, and the velocity of the vibration of the beam, the frequency response function (FRF) was estimated using a H_1 spectral estimator.[38] For this calculation, a rectangular window was used considering 10 averages of the FRFs. The stepped signal was set to sweep the range from 10 to 40 Hz with steps of 0.5 Hz during 4 s for each block to reach the steady-state response. To calculate the frequency response curve with this dataset, the level of response was recorded for each block representing the steady-state response of the system in a single frequency. Figure 3 shows the FRF and the frequency response curve to the chirp and stepped sine inputs, respectively.

In the FRF estimated with the input and output signals captured in the chirp test, it is possible to observe the distortions in the FRF as the input level is increased which is an indicative of nonlinear response since the superposition principle is not being held.[1] A clearer visualization of the nonlinear effects is possible in the stepped sine testing due to the excitation of each frequency individually during 4 s. In response to the stepped sine signal in the frequency domain, it is possible to observe the hardening effect which bends the apparent natural frequency of the system to higher values. Also, the jump-down phenomenon is visible in this response corresponding to a sudden drop in the response amplitude as the frequency of excitation is increased.

The time–frequency representation of the output for a chirp input signal estimated with a short Fourier transform is depicted in Figure 4. The black dashed lines show the harmonics of the excitation frequency. With this, it is clearly possible to observe the presence of even and odd harmonics of second and third order

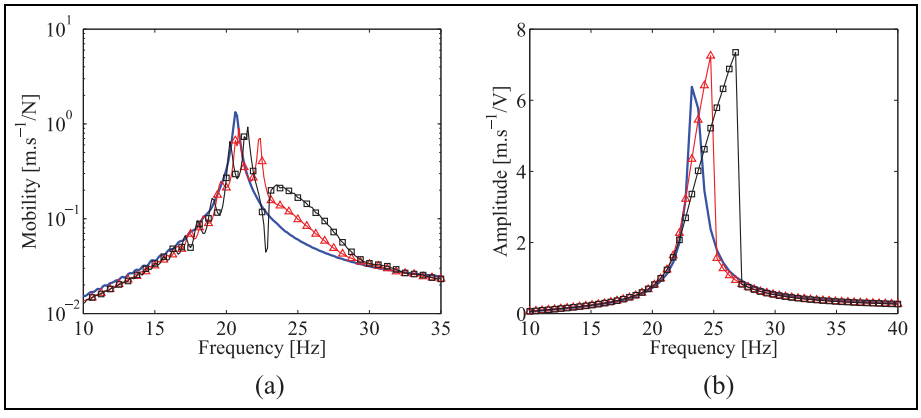

Figure 3. Detection of nonlinearity in the experimental setup. The continuous line (—) is the 0.01 V input level data, -Δ- is for 0.10 V, and -□- is for 0.15 V: (a) FRF of the system excited with a chirp excitation and (b) frequency response curve of the system excited by a stepped sine.

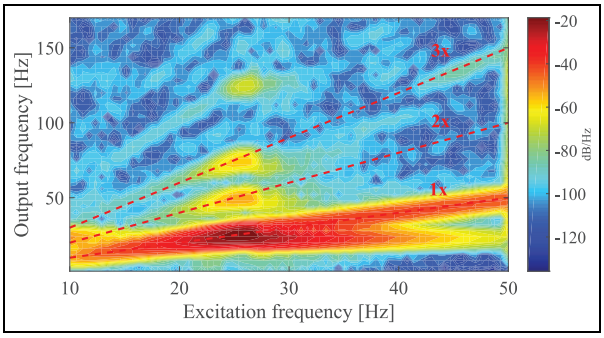

Figure 4. Time–frequency representation of the response of the system to a chirp input of 0.15 V.

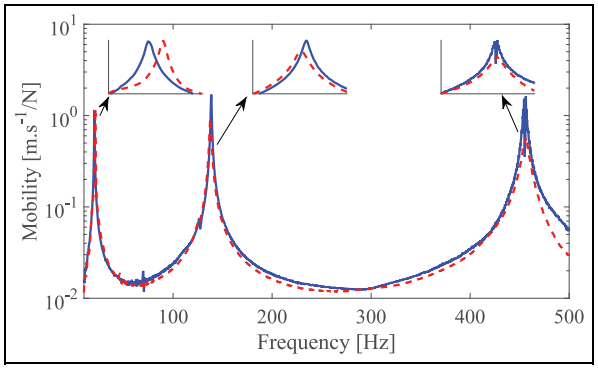

Figure 5. FRF of the experimental setup to a chirp input from 10 to 500 Hz. The continuous line (—) is the 0.01 V input level data and - - is for 0.15 V.

in the vibration of the magneto-elastic system. Higher order harmonics are also visible; however, with less significant contribution, a Volterra model is later used to represent the response of this system using the first three terms of the series expansion (y_1, y_2, and y_3). This was selected in this way because each η-order Volterra kernel is responsible of generating an ηth harmonic, respectively.[15] Truncations of the model on low orders (e.g. $\eta = 2$ or $\eta = 3$) with the Volterra expansion are common in the system identification literature. An experimental example of this is given in the paper of da Rosa et al.,[39] where the authors represent a magnetic levitation system with a fourth-order polynomial nonlinearity as a second-order Volterra model.

The vibration behavior of the nonlinear system was also verified for higher frequencies of excitation. A chirp input was applied for input voltages of 0.01 and 0.15 V with a frequency range from 10 to 500 Hz with 16,384 samples. A stepped sine was also applied in the magneto-elastic system with the same input voltage levels from 10 to 400 Hz. Figure 5 shows the FRF for the chirp input from 10 to 500 Hz and the two input levels used to excite the system. The effects in the peaks of

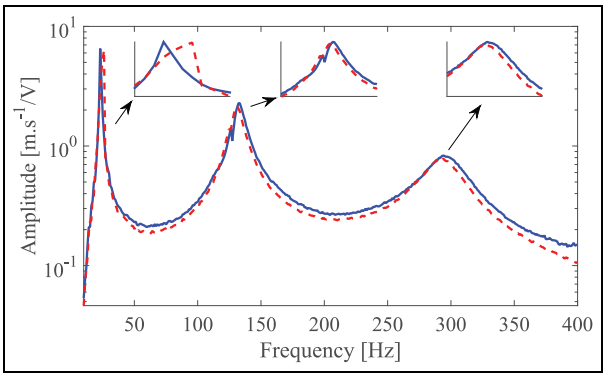

Figure 6. Frequency response curve of the experimental setup to a stepped sine input from 10 to 400 Hz. The continuous line (—) is the 0.01 V input level data and - - is for 0.15 V.

the FRFs are highlighted in this figure. It is possible to observe a hardening effect in the first mode of vibration and a softening effect due to the change of the peak to lower frequency values in the second model. Meanwhile, the nonlinear effect in the third mode is not completely clear at least in these levels of excitation. Figure 6 shows the frequency response curve for the stepped sine excitation. Similar effects as the ones found in Figure 5 can be observed with a clearer jump effect in the first natural frequency.

In this study, the chirp input dataset, which mapped the response of the magneto-elastic system around the first natural frequency, is applied to identify a Volterra model that represents the behavior of the experimental setup in the reference state.

Identification of the Volterra model

In order to represent the behavior of the nonlinear system around the first mode, it was considered a model with the first three kernels. The chirp data in the low (0.01 V) and high levels (0.15 V) were used to calculate an approximation of the Volterra kernels. The Volterra kernels were applied together with Kautz orthonormal functions[40] in order to have a reduced representation of the nonlinear model.

These Kautz functions should be selected in order to identify a proper Volterra model. For the linear kernel, it is usual to select an order $J_1 = 2$ functions since this value maintains the second-order nature of linear vibrating systems. For the selection of the orders J_2 and J_3 for the second and third kernels, respectively, a convergence analysis was performed based on the normalized root mean square error (NRMSE) between the experimental reference response y_{exp} and the output of the candidate Volterra model calculated by the multiplication of the input matrix $\mathbf{\Gamma}$ and the vector with the Volterra kernels $\mathbf{\Phi}$

Table 1. Parameters of the Kautz functions.

ω_1 (Hz)	ζ_1 (%)	ω_2 (Hz)	ζ_2 (%)	ω_3 (Hz)	ζ_3 (%)
20.65	0.65	19.03	0.27	19.91	1.38

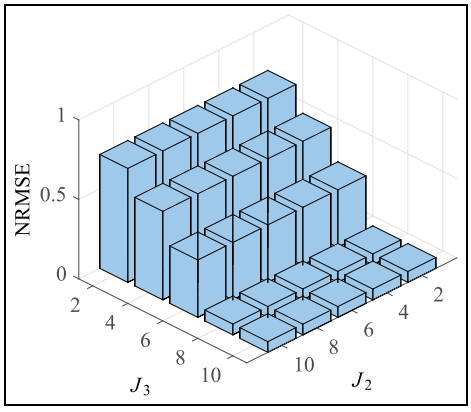

Figure 7. Convergence analysis of the orthonormal functions.

$$\text{NRMSE} = \frac{\left\| y_{exp} - \mathbf{\Gamma\Phi} \right\|}{\left\| y_{exp} - mean\left(y_{exp}\right) \right\|} s \qquad (22)$$

The calculation of the NRMSE was done by identifying the vector $\mathbf{\Phi}$ using different numbers of orthonormal functions to represent the first three Volterra kernels and calculating the output error with equation (22). This analysis is illustrated in Figure 7 for J_2 and J_3 with 2, 4, 6, 8, and 10 functions.

It is clear that the number of terms in the second kernel does not seem to modify significantly the performance of the model, while the third kernel converges the error around eight orthonormal functions. Therefore, a model with $J_1 = 2$, $J_2 = 2$, and $J_3 = 8$ orthonormal functions was considered to represent the reference state of the structure.

After the selection of the structure of the model, the parameters of the Kautz functions have to be defined. In the case of Kautz filters, these parameters are represented as complex conjugate poles that can be related to the natural frequencies and damping ratios of the system. For this study, an optimization procedure based on sequential quadratic programming (SQP) was used in order to minimize the prediction error of the model using the natural frequency and damping ratio observed in the FRF of Figure 3 as initial guesses. A more detailed description on the application of the Kautz functions for the calculation of Volterra kernels is not presented here for the sake of brevity but can be found in Shiki et al.[20] or da Silva et al.[21] Table 1 shows the frequencies (ω_η) and damping ratios (ζ_η) for each of the η-order kernels.

With the definition of the Kautz functions, it is then possible to estimate the kernels as depicted in equation (9). The orthonormal version of the model can be converted to the physical basis in order to have a visualization of this representation of the system and is illustrated in Figure 8. While the first and second kernels are fully represented, the third kernel is only partially illustrated by its main diagonal due to the additional dimension.

With the identified model, it is possible to evaluate the linear and nonlinear components of the response of the nonlinear structure. This feature is illustrated by the responses of the Volterra model with input levels corresponding to a nearly linear regime (0.01 V) and during the nonlinear regime of the system (0.15 V) as previously shown in the frequency domain in Figure 3. A direct comparison between the model response and the velocity measured in the experimental setup as well as the linear and nonlinear components of the output is illustrated in Figures 9 and 10 for the input amplitudes of 0.01 and 0.15 V, respectively.

Comparing Figures 9 and 10, it is possible to observe a clear increase in the nonlinear components relative to the linear response. This representation shows the transition between the nearly linear behavior and the nonlinear regime of motion when the displacement of the free end of the beam increases. In these figures, the nonlinear components are represented together since y_2 was not very relevant compared to y_3.

When the system is excited by a single-frequency sine input, it is possible to observe the separation of the components of the response of the model better. The nonlinear beam was excited in the linear natural frequency showing to respond with even- and odd-order harmonics. Figure 11 shows the power spectral density (PSD) of the response to the sine excitation as well as the components of the response of the model.

The PSDs clearly show that the linear component only respond in the fundamental harmonic, which is expected as a response of a simple linear system to a sine input. The second- and third-order kernels respond, respectively, with the second- and third-order harmonics that are caused by the nonlinearities in this system.

The next section shows the application of the identified model for the detection of structural variations during the linear and nonlinear regime of the setup. A comparison between a pure linear model and a

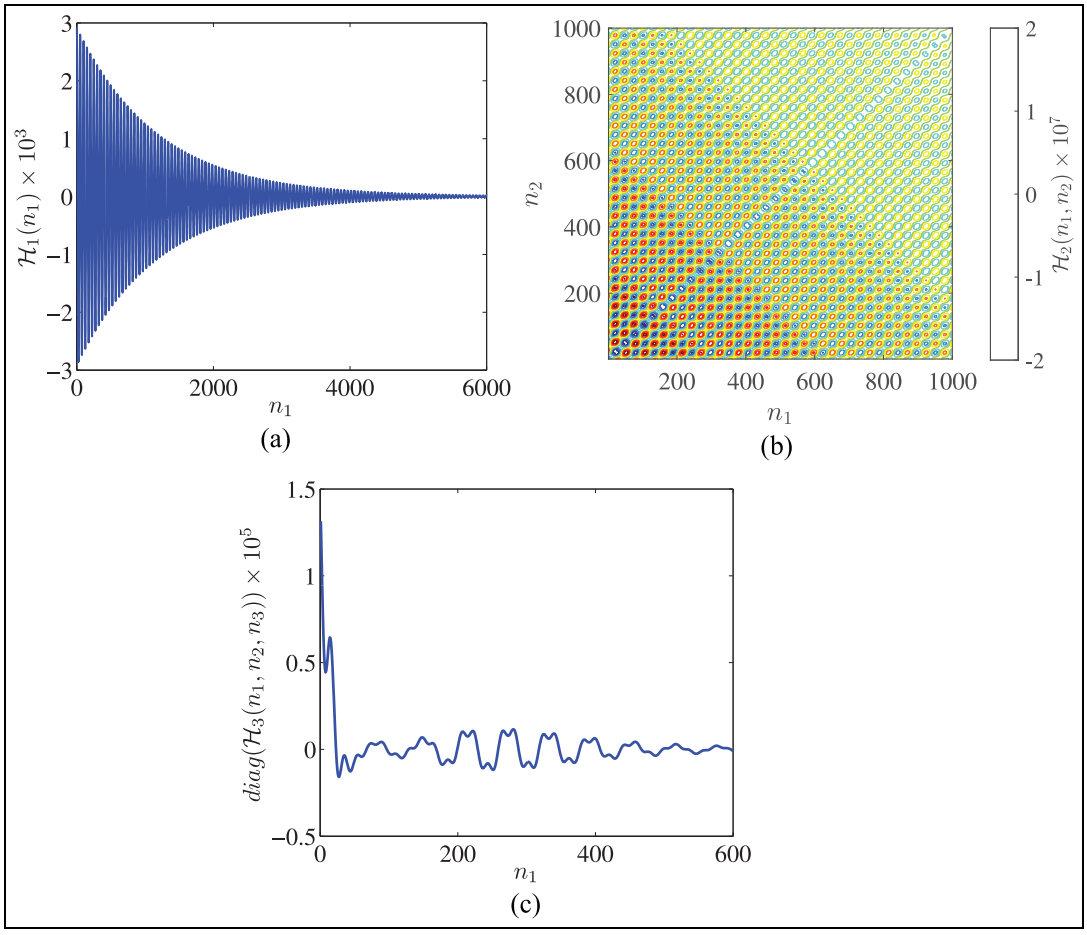

Figure 8. Representation of the Volterra kernels in the physical basis: (a) first Volterra kernel, (b) surface of the second Volterra kernel, and (c) main diagonal of the third Volterra kernel.

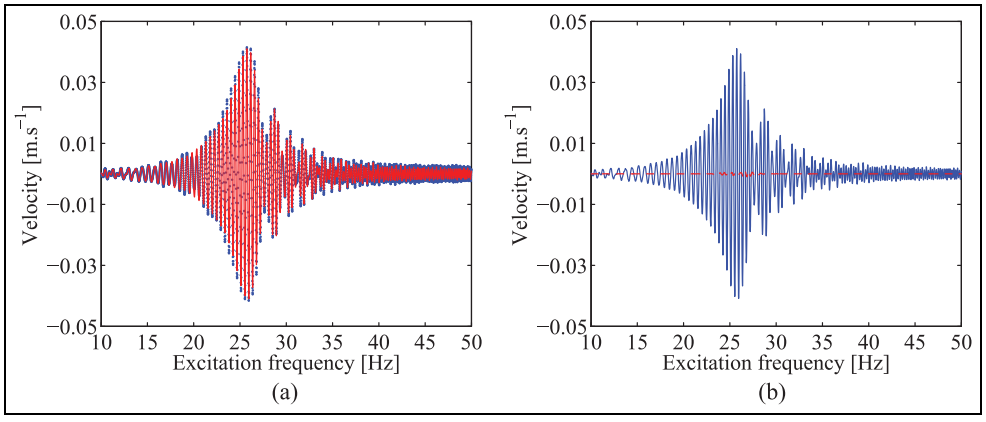

Figure 9. Response of the Volterra model to a low-level excitation (0.01 V): (a) direct comparison between the measured response (●) and the model (—) and (b) linear (—) and nonlinear (- -) components of the response.

third-order model considering the first three terms of the Volterra expansion is done in order to illustrate the problems that may arise when monitoring nonlinear structures.

Damage detection using Volterra series

In order to create structural changes in the magneto-elastic system, eight states were defined by removing up

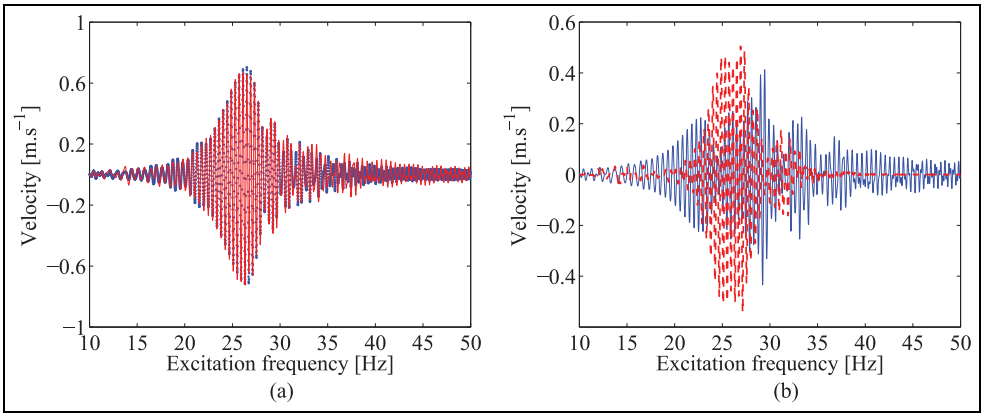

Figure 10. Response of the Volterra model to a high-level excitation (0.15 V): (a) direct comparison between the measured response (●) and the model (—) and (b) linear (—) and nonlinear (- -) components of the response.

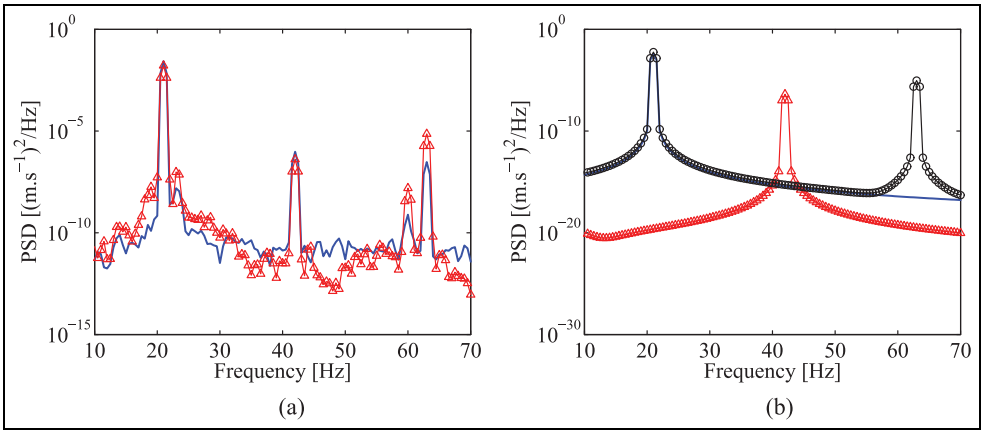

Figure 11. PSD of the response of the Volterra model to a sine excitation in the linear natural frequency of the structure: (a) PSDs of the experimental (—) and model responses (-Δ-) and (b) PSDs of the first-order (—), second-order (-Δ-), and third-order (-○-) responses.

to three masses and placing them back in the bolted connection. This was done in order to observe if the indexes showed the structure returning to the reference state by simulating a repair in the system. Each state was tested using a chirp input signal sweeping the frequencies from 10 to 50 Hz for a low-level excitation (0.01 V) and a high-level excitation (0.15 V), which represents the linear and nonlinear regime of the structure, respectively. This test was repeated 40 times in each structural condition for a better statistical characterization of the proposed damage indexes. Table 2 shows a brief description with the structural states that are simulated in the nonlinear system. Figure 12 illustrates the application of structural variation in the mass of the bolted connection.

The structural change simulated in the nonlinear system represents fundamentally a modification in a linear parameter of the system that is a concentrated mass in the bolted connection. One can argue that this option does not represent a realistic damage scenario. However, even in this case of a linear change in the system, the nonlinearity can still impose a problem if a simple linear damage feature is applied to detect

Table 2. Structural states simulated in the nonlinear system.

State	Condition
1	4 masses (reference)
2	3 masses (damaged)
3	2 masses (damaged)
4	1 mass (damaged)
5	1 mass (repair)
6	2 masses (repair)
7	3 masses (repair)
8	4 masses (repair)

modifications in the dynamic behavior. The aim in these tests is to show the lack of sensitivity of a linear damage index in comparison to an equivalent nonlinear one. The consideration of a linear structural change in the experimental results does not impose a major restriction to the methodology because even in a case where the damage causes a different kind of nonlinear behavior (e.g. breathing crack), it is expected that the prediction error–based methodology proposed in this article would still be able to indicate changes with respect to the reference state.

From the 40 repetitions of the tests, each first realization was rejected to avoid the transient response during the start of the shaker excitation resulting in 39 blocks to be analyzed. For the tested structure in this article, the most relevant response components of the Volterra series were the first- and third-order outputs y_1 and y_3 as already mentioned in the previous sections. Considering this fact, the indexes λ_1 and λ_3 were calculated in order to observe the differences between the performance of a linear and a nonlinear model in the monitoring of the test structure. Figures 13 and 14 show the linear and nonlinear indexes, respectively, for the low-level input (0.01 V) and high-level input (0.15 V). While the blue continuous line represents the indexes through the progress of the damage from states 1 to 4, the red dashed line shows the simulation of the repair of the system to the reference condition from states 5 to 8 (see Table 2). The vertical black dashed lines separate the indexes obtained from different numbers of masses placed in the bolted connection.

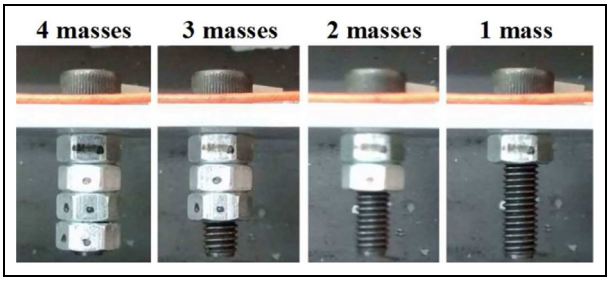

Figure 12. Illustration of the damage simulation.

In the linear damage index λ_1 shown in Figure 13, it is possible to observe a clear separation between the calculated indexes for each structural state only when the input level is low. For this situation, the linear model represented by the first Volterra kernel is already enough for an accurate detection of the outliers that appear due to the damage since there is no significant nonlinear behavior at this level of excitation. When the input is increased to 0.15 V in the shaker, λ_1 starts to have a poor performance and it is not possible to observe a clear difference between each state. At an excitation of 0.15 V, the nonlinear components start to play an important role in the total response of the system. In this way, the nonlinearity in the response of the system can mask dynamical effects that may come from damages in the system.

However, observing the nonlinear index λ_3 that takes into account the first three Volterra kernels, it is possible to observe a good separation between the states both in the low and high level input. These results clearly show the need of an appropriate nonlinear model to detect variations when nonlinearity is present before the damage.

Instead of only relying on the inspection of the indexes illustrated in Figures 13 and 14, the statistical hypothesis test depicted in equation (20) can be applied. Figures 15 and 16 show a comparison between the histogram of the calculated indexes against the theoretical

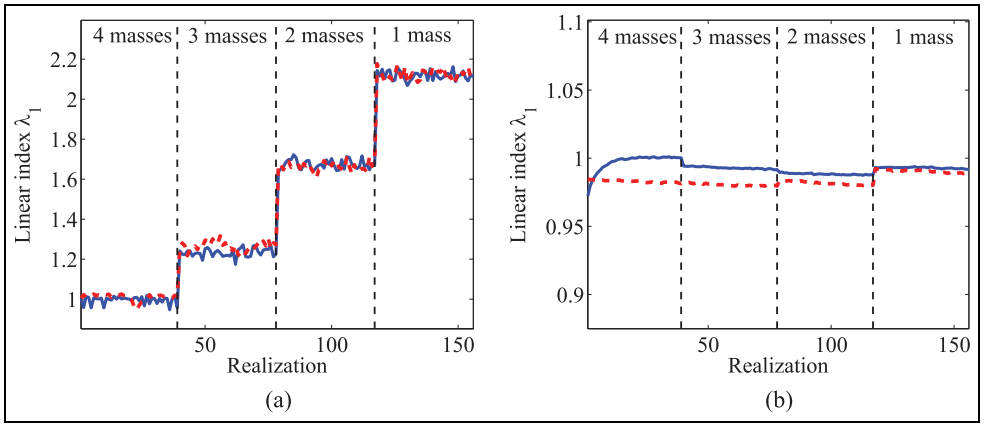

Figure 13. Linear index under two different input levels. The continuous line (—) is representing the indexes during the damage application (states 1–4) and - - represents the indexes during the repair (states 5–8): (a) low-level input (0.01 V) and (b) high-level input (0.15 V).

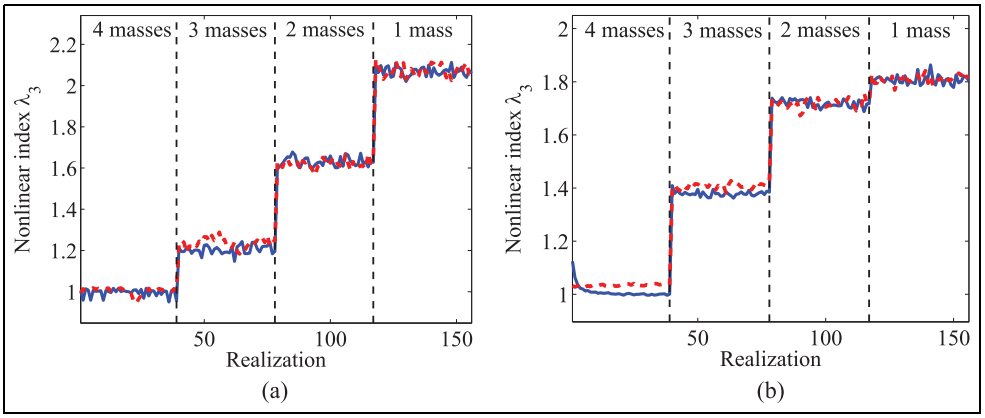

Figure 14. Nonlinear index under two different input levels. The continuous line (—) is representing the indexes during the damage application (states 1–4) and - - represents the indexes during the repair (states 5–8): (a) low-level input (0.01 V) and (b) high-level input (0.15 V).

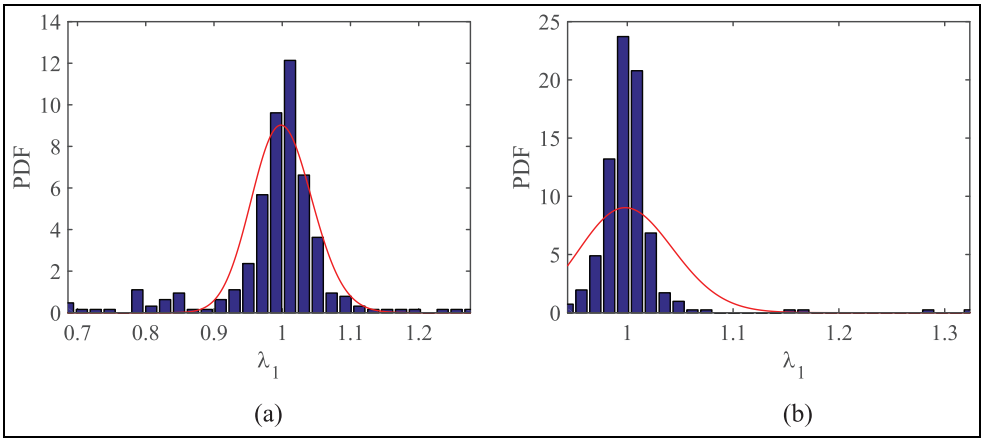

Figure 15. Distribution of the experimental linear damage index compared to the theoretical distribution for the reference case. The blue bar represents the experimental data and the continuous line (—) represents the theoretical distribution: (a) low-level input (0.01 V) and (b) high-level input (0.15 V).

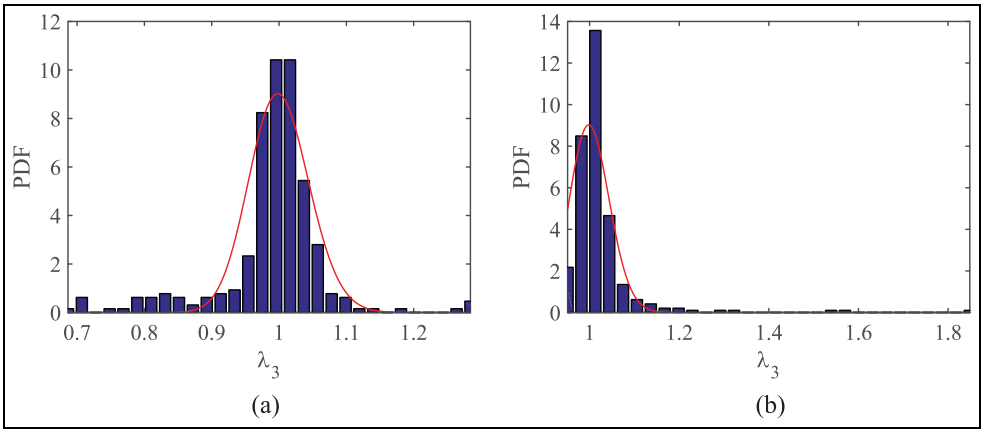

Figure 16. Distribution of the experimental nonlinear damage index compared to the theoretical distribution for the reference case. The blue bar represents the experimental data and the continuous line (—) represents the theoretical distribution: (a) low-level input (0.01 V) and (b) high-level input (0.15 V).

Table 3. Results of the hypothesis tests for different significance levels under low-level input (0.01 V).

α (%)	Linear index (λ_1)		Nonlinear index (λ_3)	
	False alarm (%)	True detection (%)	False alarm (%)	True detection (%)
2	0	100	0	100
1	0	100	0	100
0.5	0	100	0	100

Table 4. Results of the hypothesis tests for different significance levels under high-level input (0.15 V).

α (%)	Linear index (λ_1)		Nonlinear index (λ_3)	
	False alarm (%)	True detection (%)	False alarm (%)	True detection (%)
2	0	0	34.6	100
1	0	0	17.9	100
0.5	0	0	3.85	100

distribution presented in equation (18). These distributions represent the reference state of the nonlinear system that is being studied. Since there are only 39 samples of the index during the reference state, these indexes were resampled to 312 by taking fractions of the whole prediction error.

From these figures, it is clear that most of the histograms tend to follow the theoretical distribution. The exception is in the case of the linear index for a high-level input (Figure 15(b)) where the discrepancy between the data and the distribution is visible. This difference was already expected since the underlying linear model is inappropriate to represent the response of the structure during the nonlinear regime.

Tables 3 and 4 show the percentages of false alarms and true detections based on the results of the hypothesis tests for the datasets considering the excitation of 0.01 and 0.15 V, respectively. The results are illustrated for the linear and nonlinear indexes for significance levels α of 2%, 1%, and 0.5%. With these significance levels, the thresholds in terms of the damage index are $\lambda_{2\%} = 1.033$, $\lambda_{1\%} = 1.037$, and $\lambda_{0.5\%} = 1.041$, respectively. These values represent the limit values for which the system is still considered to be in the reference condition in a way that any higher values of the index λ will be considered to represent a change in the structural state. The threshold values also illustrate the fact that α is the probability of false detection since for higher significance levels the likelihood of false alarms is increased.

In Table 3, for a low-level input, both λ_1 and λ_3 perform in the same way since the nonlinear components are not strong for the 0.01 V input level. In this case, there were no false alarms and all damaged outliers were correctly classified. This happened because at this level of excitation the damaged λ_η indexes showed to be very well separated from the indexes in the reference state, which were around one as it was possible to observe in Figures 13(a) and 14(a).

Table 4 depicts the results of the damage indexes during the nonlinear regime of motion. It is clear that the linear model λ_1 is not only sensitive to structural variations when nonlinearity is present but also there is no register of false alarms in this index. The λ_3 index successfully classifies all the damaged cases for the investigated significance levels. However, a few false alarms are observed mainly because the indexes calculated in states 1 and 8 during the repair have some differences (see Figure 14(b)). This problem can be minimized by decreasing the significance level of the hypothesis test. From Table 4, it was observed that it is possible to decrease the false alarms from 34.6% to 3.85% by changing α from 2% to 0.5%. Since the variable λ_3 is quite sensitive to structural variations and the values of the damaged states are relatively far from the reference (see Figures 13 and 14), it is possible to select a very low value of α which minimizes the probability of false positives.

In order to analyze how the classification index works under different values of α, it is possible to map many values of this parameter in a receiver-operating characteristic (ROC) curve. This presents the false alarm rates against the true detection rates for many values of thresholds for the binary classification, which in this article is represented by the significance level α of the hypothesis test. Figure 17 shows the ROC curves for the results of the linear and nonlinear indexes under the excitation levels of 0.01 and 0.15 V.

The linear index λ_1 shows to have a good detection rate in the low-level input but significantly lose performance when the excitation level is increased. During the

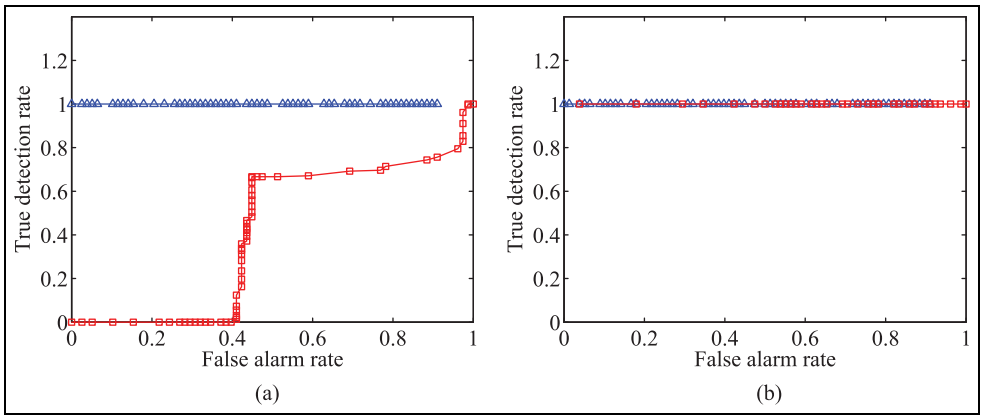

Figure 17. ROC curves of the damage indexes. -Δ- is the curve for the low-level input (0.01 V) and -□- is the curve for the high-level input (0.15 V): (a) linear index and (b) nonlinear index.

high-level input, λ_1 can have a performance close to a random classifier. Meanwhile, the nonlinear index λ_3 has a good detection rate during both input levels and the false alarms can be minimized by setting lower values for the significance level of the test.

Final remarks

In this article, the discrete version of the Volterra model was applied to represent the behavior of a magneto-elastic nonlinear system in the reference condition. A damage index based on the prediction error of the model was used to detect structural variations in the system during the linear and nonlinear regime of motion. The nonlinear index was able to detect structural changes in both regimes of motion, while the linear version of the damage indicator failed during the nonlinear regime. These results showed that nonlinear behavior can mask effects of damage when a proper model is not used. Although the simulated damage represented mostly a variation in a linear parameter (a concentrated mass), the nonlinear index was still necessary for an accurate detection. If the structural change revealed some nonlinear feature of the system, it is likely that the method would still correctly classify the state of the system since it is based on a model representing the nonlinear behavior of the system in the reference condition. This means that any other unaccounted phenomenon will be seen as an outlier by the statistical classification.

This conclusion was possible because of the fact that Volterra series is a generalization of the linear convolution model allowing one to directly compare a nonlinear index with its equivalent linear version. However, it is possible that for higher levels of excitation even the nonlinear index can fail since higher order nonlinearities can appear in a way that more terms in the Volterra expansion may be necessary. This is still a common problem in nonlinear systems since it is difficult to have general models to represent the whole nonlinear behavior. Another possible drawback of the presented technique is the need of both input and output signals to apply the method as well as a test made during the reference condition of the system to define the baseline.

Even though the results and conclusions were made with damage features based on Volterra series, it is possible to conclude that any linear model could have problems when trying to detect variations in the behavior of a nonlinear structure. Even in the case when it is considered that the damage is the source of nonlinear behavior, some false positives are expected if the inherent nonlinearities of the system are not taken into account. This shows the importance of nonlinearity identification before using damage detection techniques since a prior knowledge about the behavior of the system can help in a decision about taking or not some efforts on nonlinear modeling.

Declaration of Conflicting Interests

The author(s) declared no potential conflicts of interest with respect to the research, authorship, and/or publication of this article.

Funding

The author(s) disclosed receipt of the following financial support for the research, authorship, and/or publication of this article: The first and second authors acknowledge the financial support provided by São Paulo Research Foundation (FAPESP, Brasil) by the grant number 12/09135-3 and the National Council for Scientific and Technological Development (CNPq, Brasil) by the grant number 470582/2012-0. The first author is thankful to FAPESP for his doctorate scholarship grant number 13/25148-0 and the research internships abroad program (Bolsa Estágio de Pesquisa no Exterior (BEPE)) grant number 15/03560-2, which allowed

him to work in University of California, San Diego under the supervision of Prof. Todd.

References

1. Worden K and Tomlinson GR. *Nonlinearity in structural dynamics*. London: Institute of Physics Publishing, 2001.
2. Kerschen G, Worden K, Vakakis AF, et al. Past, present and future of nonlinear system identification in structural dynamics. *Mech Syst Signal Pr* 2006; 20: 502–592, http://www.sciencedirect.com/science/article/pii/S0888327005000828
3. Virgin LN. *Introduction to experimental nonlinear dynamics: a case study in mechanical vibration*. Cambridge University Press, 2000, http://books.google.com.br/books?id = L8dLzjTpyhAC
4. Farrar CR, Worden K, Todd MD, et al. *Nonlinear system identification for damage detection*. Los Alamos, NM: Los Alamos National Laboratory, 2007.
5. Nichols JM and Todd MD. Nonlinear features for SHM applications. In: *Encyclopedia of structural health monitoring*. John Wiley & Sons, Ltd, 2009, http://dx.doi.org/10.1002/9780470061626.shm049
6. Overbey LA and Todd MD. Analysis of local state space models for feature extraction in structural health monitoring. *Struct Health Monit* 2007; 6(2): 145–172, http://shm.sagepub.com/content/6/2/145.abstract
7. Worden K, Farrar CR, Haywood J, et al. A review of nonlinear dynamics applications to structural health monitoring. *Struct Control Hlth* 2008; 15(4): 540–567, http://dx.doi.org/10.1002/stc.215
8. Bandara RP, Chan TH and Thambiratnam DP. Structural damage detection method using frequency response functions. *Struct Health Monit* 2014, http://shm.sagepub.com/content/early/2014/02/19/1475921714522847.abstract
9. Yelve NP, Mitra M and Mujumdar PM. Spectral damage index for estimation of breathing crack depth in an aluminum plate using nonlinear Lamb wave. *Struct Control Hlth* 2014; 21(5): 833–846, http://dx.doi.org/10.1002/stc.1604
10. Mohammadi Ghazi R and Büyüköztürk O. Damage detection with small data set using energy-based nonlinear features. *Struct Control Hlth* 2016, http://dx.doi.org/10.1002/stc.1774
11. Bornn L, Farrar CR and Park G. Damage detection in initially nonlinear systems. *Int J Eng Sci* 2010; 48(10): 909–920, http://www.sciencedirect.com/science/article/pii/S0020722510001059
12. Chanpheng T, Yamada H, Katsuchi H, et al. Nonlinear features for damage detection on large civil structures due to earthquakes. *Struct Health Monit* 2012; 11(4): 482–488, http://shm.sagepub.com/content/11/4/482.abstract
13. Reynders E, Wursten G and De Roeck G. Output-only structural health monitoring in changing environmental conditions by means of nonlinear system identification. *Struct Health Monit* 2013; 13: 82–93, http://shm.sagepub.com/content/early/2013/10/29/1475921713502836.abstract
14. Rugh WJ. *Nonlinear system theory—the Volterra/Wiener approach*. Baltimore, MD: The Johns Hopkins University Press, 1991.
15. Schetzen M. *The Volterra and Wiener theories of nonlinear systems*. New York: John Wiley & Sons, 1980.
16. Carassale L and Kareem A. Synthesis of multi-variate Volterra systems by a topological assemblage scheme. *Probabilist Eng Mech* 2014; 37: 109–122, http://www.sciencedirect.com/science/article/pii/S0266892014000447
17. Kim Y. Prediction of the dynamic response of a slender marine structure under an irregular ocean wave using the NARX-based quadratic Volterra series. *Appl Ocean Res* 2015; 49: 42–56, http://www.sciencedirect.com/science/article/pii/S0141118714001138
18. Chatterjee A. Structural damage assessment in a cantilever beam with a breathing crack using higher order frequency response functions. *J Sound Vib* 2010; 329(16): 3325–3334, http://www.sciencedirect.com/science/article/pii/S0022460X10001495
19. Silva W. Identification of nonlinear aeroelastic systems based on the Volterra theory: progress and opportunities. *Nonlinear Dynam* 2005; 39(1–2): 25–62, http://dx.doi.org/10.1007/s11071-005-1907-z
20. Shiki SB, Lopes V Jr and da Silva S. Identification of nonlinear structures using discrete-time Volterra series. *J Braz Soc Mech Sci* 2014, http://dx.doi.org/10.1007/s40430-013-0088-9
21. da Silva S, Cogan S and Foltête E. Nonlinear identification in structural dynamics based on Wiener series and Kautz filters. *Mech Syst Signal Pr* 2010; 24(1): 52–58, http://www.sciencedirect.com/science/article/pii/S0888327009001897
22. da Silva S. Non-linear model updating of a three-dimensional portal frame based on Wiener series. *Int J Nonlin Mech* 2011; 46(1): 312–320, http://www.sciencedirect.com/science/article/pii/S0020746210001472
23. Shiki SB, Lopes V Jr and da Silva S. Damage detection in nonlinear structures using discrete-time Volterra series. *Key Eng Mat* 2013; 569: 876–883, www.scientific.net/KEM.569-570.876
24. Tawfiq I and Vinh T. Contribution to the extension of modal analysis to non-linear structure using Volterra functional series. *Mech Syst Signal Pr* 2003; 17(2): 379–407, http://www.sciencedirect.com/science/article/pii/S0888327002914998
25. Cheng CM, Peng ZK, Zhang WM, et al. Wavelet basis expansion-based Volterra kernel function identification through multilevel excitations. *Nonlinear Dynam* 2014; 76(2): 985–999, http://dx.doi.org/10.1007/s11071-013-1182-3
26. Ruotolo R, Surace C, Crespo P, et al. Harmonic analysis of the vibrations of a cantilevered beam with a closing crack. *Comput Struct* 1996; 61(6): 1057–1074, http://www.sciencedirect.com/science/article/pii/0045794996001848
27. Peng ZK, Lang ZQ, Chu FL, et al. Locating nonlinear components in periodic structures using nonlinear effects. *Struct Health Monit* 2010; 9(5): 401–411, http://shm.sagepub.com/content/9/5/401.abstract

28. Surace C, Ruotolo R and Storer D. Detecting nonlinear behavior using the Volterra series to assess damage in beam-like structures. *J Theor Appl Mech* 2011; 49: 905–926.
29. Rébillat M, Hajrya R and Mechbal N. Nonlinear structural damage detection based on cascade of Hammerstein models. *Mech Syst Signal Pr* 2014; 48(1–2): 247–259, http://www.sciencedirect.com/science/article/pii/S0888327014000843
30. Tang H, Liao YH, Cao JY, et al. Fault diagnosis approach based on Volterra models. *Mech Syst Signal Pr* 2010; 24(4): 1099–1113, http://www.sciencedirect.com/science/article/pii/S0888327009002611
31. Doyle F III, Pearson RK and Ogunnaike BA. *Identification and control using Volterra models*. London: Springer, 2012, https://books.google.com/books?id=w5HxBwAAQBAJ
32. Zanos TP, Courellis SH, Berger TW, et al. Nonlinear modeling of causal interrelationships in neuronal ensembles. *IEEE Trans Neural Syst Rehabil Eng* 2008; 16(4): 336–352.
33. Phukpattaranont P and Ebbini ES. Post-beamforming second-order Volterra filter for pulse-echo ultrasonic imaging. *IEEE Trans Ultrason Ferroelectr Freq Control* 2003; 50(8): 987–1001.
34. Heuberger PSC, van der Hof PMJ and Wahlberg B. *Modelling and identification with rational orthogonal basis functions*. Berlin: Springer, 2005.
35. Sohn H and Farrar CR. Damage diagnosis using time series analysis of vibration signals. *Smart Mater Struct* 2001; 10(3): 446, http://stacks.iop.org/0964-1726/10/i=3/a=304
36. Bendat JS and Piersol AG. *Random data: analysis and measurement procedures*. John Wiley & Sons, 2011, https://books.google.com/books?id=qYSViFRNMlwC
37. Hogg RV and Ledolter J. *Engineering statistics*. Macmillan, 1987, http://books.google.com.br/books?id=jIIoAQAAMAAJ
38. Stoica P and Moses RL. *Spectral analysis of signals*. Pearson Prentice Hall, 2005, http://books.google.com.br/books?id=h78ZAQAAIAAJ
39. da Rosa A, Campello RJGB and Amaral WC. Exact search directions for optimization of linear and nonlinear models based on generalized orthonormal functions. *IEEE Trans Automat Contr* 2009; 54(12): 2757–2772.
40. Kautz WH. Transient synthesis in the time domain. *IRE Trans Circuit Theory* 1954; CT-1: 29–39.

Appendix 1

Calculation of the matrix form of the Volterra series

As previously presented, considering the orthonormal expansion of the Volterra kernels the η-order response $y_\eta(k)$ is given by

$$y_\eta(k) \approx \sum_{i_1=1}^{J_\eta-1} \cdots \sum_{i_\eta=1}^{J_\eta-1} \mathcal{B}_\eta(i_1, \ldots, i_\eta) \prod_{j=1}^{\eta} l_{i_j}(k) \tag{23}$$

where $\mathcal{B}_\eta(i_1, \ldots, i_\eta)$ are the orthonormal projections of the Volterra kernels, $J_1, \ldots, J_\eta$ are the number of samples in each orthonormal projection, and $l_{i_j}(k)$ is the filtered input signal. To demonstrate the formulation of the model in the matrix form, it was considered a model of order $\eta = 3$ without loss of generality since for higher orders the procedure should follow the same idea. In this case, the first three components of the Volterra series expansion are given by

$$y_1(k) = \sum_{i_1=0}^{J_1-1} \mathcal{B}_1(i_1) l_{i_1}(k) \tag{24}$$

$$y_2(k) = \sum_{i_1=0}^{J_2-1} \sum_{i_2=0}^{J_2-1} \mathcal{B}_2(i_1, i_2) l_{i_1}(k) l_{i_2}(k) \tag{25}$$

$$y_3(k) = \sum_{i_1=0}^{J_3-1} \sum_{i_2=0}^{J_3-1} \sum_{i_3=0}^{J_3-1} \mathcal{B}_3(i_1, i_2, i_3) l_{i_1}(k) l_{i_2}(k) l_{i_3}(k) \tag{26}$$

where $y_1(k)$, $y_2(k)$, and $y_3(k)$ are the first-, second-, and third-order components, respectively, $\mathcal{B}_1(i_1)$, $\mathcal{B}_2(i_1, i_2)$, and $\mathcal{B}_3(i_1, i_2, i_3)$ are the first-, second-, and third-order kernels in the orthonormal domain, and $l_{i_1}(k)$, $l_{i_2}(k)$, and $l_{i_3}(k)$ are the filtered input signals. Since the Volterra model is linear with respect to the parameters, it is possible to write the vector with the collection of the η-order responses ($\mathbf{y}_\eta$) as

$$\mathbf{y}_\eta = \mathbf{\Gamma}_\eta \mathbf{\Phi}_\eta \tag{27}$$

where $\mathbf{\Gamma}_\eta$ is a matrix with the input signal filtered by the orthonormal functions representing the ηth kernel and $\mathbf{\Phi}_\eta$ is a vector with the collection of the unique terms in the ηth orthonormal kernel. The vector $\mathbf{y}_\eta$ can be written as a vector with the samples of the ηth output of the Volterra expansion

$$\mathbf{y}_\eta = [\, y_\eta(0) \quad y_\eta(1) \quad \ldots \quad y_\eta(k) \,]^T \tag{28}$$

With the definition of the η-order output vector, it is necessary to define the matrices $\mathbf{\Gamma}_\eta$ and $\mathbf{\Phi}_\eta$. For the first-order term of the Volterra model, the kth row of the matrix $\mathbf{\Gamma}_1$ can be given by

$$\mathbf{\Gamma_1}(k,:) = \begin{bmatrix} l_0(k) & l_1(k) & \ldots & l_{i_j}(k) \end{bmatrix} \tag{29}$$

The vector $\mathbf{\Phi}_1$ with the unique terms of the first-order orthonormal kernel is

$$\mathbf{\Phi_1} = [\, \mathcal{B}_1(0) \quad \mathcal{B}_1(1) \quad \ldots \quad \mathcal{B}_1(i_1) \,]^T \tag{30}$$

Note that in the case of the first-order kernel, all the terms are considered in the vector $\mathbf{\Phi}_1$ since they are all unique.

In a similar way, for the second-order terms, the kth row of the matrix $\mathbf{\Gamma}_2$ can be given by

$$\boldsymbol{\Phi}_3 = [\,\mathcal{B}_3(0,0,0) \quad \mathcal{B}_3(1,0,0) \quad \mathcal{B}_3(1,1,0) \quad \mathcal{B}_3(1,1,1) \quad \mathcal{B}_3(2,0,0) \quad \mathcal{B}_3(2,1,0) \quad \ldots \quad \ldots \quad \mathcal{B}_3(2,2,2) \quad \ldots \quad \mathcal{B}_3(i_1,0,0) \quad \ldots \quad \mathcal{B}_3(i_1,i_2,i_3)\,]^T \tag{34}$$

$$\boldsymbol{\Gamma}_2(k,\,:) = \left[\, l_0(k)^2 \quad 2l_1(k)l_0(k) \quad l_1(k)^2 \quad \ldots \quad 2l_{i_j}(k)l_0(k) \quad \ldots \quad l_{i_j}(k)^2 \,\right] \tag{31}$$

and the vector $\boldsymbol{\Phi}_2$ is written as

$$\boldsymbol{\Phi}_2 = [\,\mathcal{B}_2(0,0) \quad \mathcal{B}_2(1,0) \quad \mathcal{B}_2(1,1) \quad \ldots \quad \mathcal{B}_2(i_1,0) \quad \ldots \quad \mathcal{B}_2(i_1,i_2)\,]^T \tag{32}$$

Note that a few terms in the matrix $\boldsymbol{\Gamma}_2$ are multiplied by a constant integer number since they appear multiple times in the response. Also, only the terms in the main diagonal and below are taken into account in $\boldsymbol{\Phi}_2$ since it is considered that the kernels are symmetric.

For the third-order component, the kth row of the matrix $\boldsymbol{\Gamma}_3$ is written as

$$\boldsymbol{\Gamma}_3(k,:) = \left[\, l_0(k)^3 \quad 3l_1(k)l_0(k)^2 \quad 3l_1(k)^2l_0(k) \quad l_1(k)^3 \quad 6l_2(k)l_1(k)l_0(k) \quad \ldots \quad \ldots \quad l_2(k)^3 \quad \ldots \quad 3l_{i_j}(k)l_0(k)^2 \quad \ldots \quad l_{i_j}(k)^3 \,\right] \tag{33}$$

and the vector $\boldsymbol{\Phi}_3$ with the unique terms in the third-order kernel is

Considering the Volterra expansion until the order $\eta = 3$, the resultant input matrix $\boldsymbol{\Gamma}$ is given by combining the $\boldsymbol{\Gamma}_\eta$ matrices

$$\boldsymbol{\Gamma} = [\,\boldsymbol{\Gamma}_1 \quad \boldsymbol{\Gamma}_2 \quad \boldsymbol{\Gamma}_3\,] \tag{35}$$

And the vector $\boldsymbol{\Phi}$ with the unique terms of the Volterra kernels is written as

$$\boldsymbol{\Phi} = [\,\boldsymbol{\Phi}_1 \quad \boldsymbol{\Phi}_2 \quad \boldsymbol{\Phi}_3\,]^T \tag{36}$$

In the case where it is necessary to estimate the Volterra kernels with the knowledge of the input signal (i.e. the matrix $\boldsymbol{\Gamma}$) and the measured output (i.e. the vector $\mathbf{y}$), one should compute $\boldsymbol{\Gamma}$ and $\mathbf{y}$ and then estimate the Volterra kernels through the least-squares approximation

$$\boldsymbol{\Phi} = \left(\boldsymbol{\Gamma}^T\boldsymbol{\Gamma}\right)^{-1}\boldsymbol{\Gamma}^T\mathbf{y} \tag{37}$$